Journal of Neural Engineering

PAPER

Independent component analysis for cochlear implant artifacts attenuation from electrically evoked auditory steady-state response measurements

To cite this article: Hanne Deprez *et al* 2018 *J. Neural Eng.* **15** 016006

View the article online for updates and enhancements.

Related content

- Single-trial event-related potential extraction through one-unit ICA-with-reference
Wee Lih Lee, Tele Tan, Torbjörn Falkmer et al.
- Using independent component analysis to remove artifacts in visual cortex responses elicited by electrical stimulation of the optic nerve
Yiliang Lu, Pengjia Cao, Jingjing Sun et al.
- EEG artifact removal—state-of-the-art and guidelines
Jose Antonio Urigüen and Begoña Garcia-Zapirain

PITT | SWANSON ENGINEERING
BIOENGINEERING

The Department of Bioengineering at the University of Pittsburgh Swanson School of Engineering invites applications from accomplished individuals with a PhD or equivalent degree in bioengineering, biomedical engineering, or closely related disciplines for an open-rank, tenured/tenure-stream faculty position. We wish to recruit an individual with strong research accomplishments in Translational Bioengineering (i.e., leveraging basic science and engineering knowledge to develop innovative, translatable solutions impacting clinical practice and healthcare), with preference given to research focus on neuro-technologies, imaging, cardiovascular devices, and biomimetic and biorobotic design. It is expected that this individual will complement our current strengths in biomechanics, bioimaging, molecular, cellular, and systems engineering, medical product engineering, neural engineering, and tissue engineering and regenerative medicine. In addition, candidates must be committed to contributing to high quality education of a diverse student body at both the undergraduate and graduate levels.

CLICK HERE FOR FURTHER DETAILS

To ensure full consideration, applications must be received by June 30, 2019. However, applications will be reviewed as they are received. Early submission is highly encouraged.

This content was downloaded from IP address 134.58.253.56 on 01/08/2019 at 11:04

IOP Publishing Journal of Neural Engineering
J. Neural Eng. **15** (2018) 016006 (17pp) https://doi.org/10.1088/1741-2552/aa87ce

Independent component analysis for cochlear implant artifacts attenuation from electrically evoked auditory steady-state response measurements

Hanne Deprez[1,2], Robin Gransier[2], Michael Hofmann[2], Astrid van Wieringen[2], Jan Wouters[2] and Marc Moonen[1]

[1] STADIUS Center for Dynamical Systems, Signal Processing and Data Analytics, Department of Electrical Engineering (ESAT), KU Leuven, Kasteelpark Arenberg 10 bus 2440, 3001 LEUVEN, Belgium
[2] Experimental ORL, Department of Neurosciences, KU Leuven, Herestraat 49 bus 721, 3000 LEUVEN, Belgium

E-mail: hanne.deprez@esat.kuleuven.be

Received 19 January 2017, revised 8 June 2017
Accepted for publication 23 August 2017
Published 6 December 2017

Abstract

Objective. Electrically evoked auditory steady-state responses (EASSRs) are potentially useful for objective cochlear implant (CI) fitting and follow-up of the auditory maturation in infants and children with a CI. EASSRs are recorded in the electro-encephalogram (EEG) in response to electrical stimulation with continuous pulse trains, and are distorted by significant CI artifacts related to this electrical stimulation. The aim of this study is to evaluate a CI artifacts attenuation method based on independent component analysis (ICA) for three EASSR datasets. *Approach.* ICA has often been used to remove CI artifacts from the EEG to record transient auditory responses, such as cortical evoked auditory potentials. Independent components (ICs) corresponding to CI artifacts are then often manually identified. In this study, an ICA based CI artifacts attenuation method was developed and evaluated for EASSR measurements with varying CI artifacts and EASSR characteristics. Artifactual ICs were automatically identified based on their spectrum. *Main results.* For 40 Hz amplitude modulation (AM) stimulation at comfort level, in high SNR recordings, ICA succeeded in removing CI artifacts from all recording channels, without distorting the EASSR. For lower SNR recordings, with 40 Hz AM stimulation at lower levels, or 90 Hz AM stimulation, ICA either distorted the EASSR or could not remove all CI artifacts in most subjects, except for two of the seven subjects tested with low level 40 Hz AM stimulation. Noise levels were reduced after ICA was applied, and up to 29 ICs were rejected, suggesting poor ICA separation quality. *Significance.* We hypothesize that ICA is capable of separating CI artifacts and EASSR in case the contralateral hemisphere is EASSR dominated. For small EASSRs or large CI artifact amplitudes, ICA separation quality is insufficient to ensure complete CI artifacts attenuation without EASSR distortion.

Keywords: cochlear implant (CI), CI artifacts attenuation, electrically evoked auditory steady-state response (EASSR), independent component analysis

(Some figures may appear in colour only in the online journal)

 © 2017 IOP Publishing Ltd Printed in the UK

1. Introduction

Cochlear implants (CIs) can partially restore hearing in severely to profoundly hearing impaired subjects by electrically stimulating the auditory nerve with electrical pulse trains. The internal part consists of an electrode array with 12–22 electrodes inserted in the cochlea, and one or two extra-cochlear electrodes. Stimulation channels are either between two intra-cochlear electrodes (i.e. bipolar mode (BP)), or between an intra-cochlear and an extra-cochlear electrode (i.e. monopolar mode (MP)). Clinically, high-rate stimulation is used, i.e. $\geqslant$500 pulses per second (pps) [1]. Furthermore, MP stimulation is typically used to save battery life, as it requires less current than BP stimulation to elicit an equal loudness percept [2].

Prior to CI switch-on and during rehabilitation, minimum and maximum electrical stimulation levels (T and C levels), which vary across stimulation channels and CI subjects, must be determined during CI fitting. With MP stimulation, T and C levels vary less across stimulation channels compared to BP stimulation, which is another reason that MP stimulation is clinically preferred. T and C levels are typically determined based on behavioral feedback, that is not easily obtained from children and subjects with additional disabilities. Objective CI fitting based on electrophysiological measures is therefore under investigation.

Electro-encephalogram (EEG) recordings, which have a high temporal and reasonable spatial resolution, have often been used to study objective CI fitting [3–5] and auditory plasticity in CI subjects [6–11]. Transient responses, i.e. electrically evoked compound action potentials (ECAPs), cortical auditory evoked potentials (CAEPs) and electrically evoked auditory brainstem responses (EABRs), as well as electrically evoked auditory steady-state responses (EASSRs) have successfully been measured in CI subjects [4, 5, 12–17].

EASSRs are potentially useful for objective CI fitting, and for studying temporal processing, auditory maturation and brain plasticity in adults and infants with a CI. (E)ASSRs are neural auditory steady-state responses, present in the EEG, which result from neural phase-locking to a periodic stimulus [18]. EASSRs can be evoked with continuous electrical stimulation [4, 5], either with unmodulated low-rate or modulated high-rate pulse trains. Modulated pulse trains are a model of the electrical pulse sequences after processing of speech by the CI processor.

EASSRs offer a number of advantages compared to transient responses. First, EASSRs are responses elicited by frequency-specific stimuli, activating one stimulation channel, compared to transient responses, which are often evoked with non-frequency specific stimuli, and with free field stimulation, activating multiple stimulation channels. Second, EASSRs can objectively be detected at f_m, e.g. using an F-test or a Hotelling T^2 test [4, 5, 19, 20], while transient responses are typically assessed subjectively by examining the latency and amplitude of visually identified peaks. Third, EASSRs can be elicited using high-rate stimulation, while the stimulation rate is limited for transient responses. T and C levels vary with stimulation rate [21, 22], and are therefore ideally determined with the clinically used stimulation rate. Although this is not impossible, it is not straightforward to record ECAPs and EABRs with clinically used stimulation rates. T levels determined with ECAPs and EABRs, using low-rate stimuli, are only moderately correlated with behavioral T levels [3, 23]. T levels determined with EASSRs, using high-rate stimulation, correlate well with behavioral T levels, at least for stimulation in BP mode [4]. The next step is to evaluate T level determination based on EASSRs for clinically used high-rate MP stimulation in MP mode.

However, the electrical stimulation produced by the CI results in electrical artifacts in the EEG (see characterization in [24]) that should be removed before further EEG signal processing. Asymmetric CI artifacts result in components at f_m, distorting the EASSR. The amount of distortion is highly subject, and stimulation parameter dependent [24]. Factors that may influence CI artifacts shape, amplitude and duration include, but are not limited to, (1) the stimulation mode, (2) the stimulation level, (3) the relative placement of stimulation electrode and ball and casing electrodes, (4) electrode-tissue interface impedance, and (5) the recording reference electrode. A CI artifacts example is given in figure 1.

CI artifacts are larger with stimulation in MP mode compared to BP mode [25, 26]. A linear interpolation (LI) method, interpolating the signal part contaminated with CI artifacts, has been used to remove CI artifacts from EASSRs with stimulation in BP mode [4, 5, 27]. This is only possible when the CI artifacts duration is shorter than the interpulse interval (IPI), i.e. the inverse of the stimulation rate f_c. It has recently been shown [24], for Cochlear Nucleus® implants, that overlapping CI artifacts are present in ipsilateral channels for 500 pps MP stimulation, and in ipsi- and contralateral recording channels for 900 pps MP stimulation. Non-overlapping CI artifacts can be removed from contralateral recording channels with LI for stimulation in MP mode with rates up to 500 pps [17, 24]. In [28] a Kalman filter has been developed that can remove non-overlapping CI artifacts from EASSRs with stimulation in BP mode at 900 pps. Recently, a template subtraction method has been proposed in [29] that has been evaluated for measurements with overlapping CI artifacts and high SNR EASSRs. In [30] an independent component analysis (ICA) based method has been presented that attenuates CI artifacts in EASSR recordings in one subject for 900 pps MP stimulation. To our knowledge, no other CI artifacts attenuation methods have been developed for EASSR recordings with overlapping CI artifacts.

For transient responses (EABRs and CAEPs), many CI artifacts attenuation methods have been proposed, and a summary is included in [24]. ICA belongs to the most investigated CI artifacts attenuation methods for transient responses, and has successfully been applied in [13–15, 31–36], although one case has also been reported where the ICA method does not produce satisfactory results [37]. The goal of ICA is to split multichannel signals in statistically independent components (ICs), that represent in this case either the EASSR, CI artifacts, ocular or muscle artifacts, or neural background noise. In most studies, ICs representing CI artifacts are manually identified based on temporal and spatial characteristics,

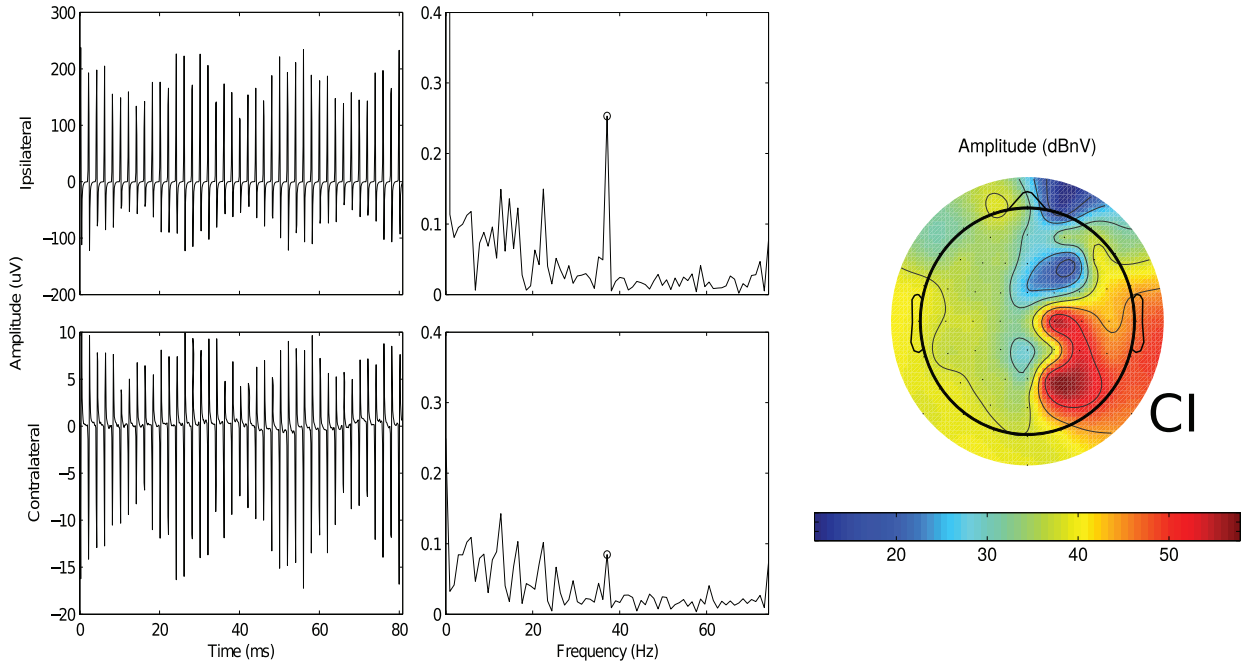


Figure 1. Example of CI artifacts for a subject, with a CI at the right side, measured with 37 Hz AM 900 pps pulse trains at a subthreshold stimulation amplitude. Left: time and frequency domain signals at recording electrodes TP_8 (ipsilateral) and TP_7 (contralateral), referenced to C_z. Right: spatial distribution of spectral power at the modulation frequency, referenced to C_z. The units of the topography plot are $\text{dBnV} = 20\ \log_{10}\ nV$, where 1 μV corresponds to 60 dBnV and 0.1 μV corresponds to 40 dBnV. No neural response is expected to be present, as subthreshold stimulation levels were used. Reprinted from [24], copyright 2017, with permission from Elsevier.

and are then rejected. Although CI artifacts are sufficiently attenuated to study the transient response, it has also been reported that residual CI artifacts are still observable [13–15]. Furthermore, CI artifacts are usually expressed on multiple ICs, ranging from 2 to 15 ICs [13, 14, 33, 38, 39]. Note, however, that the number of recording channels used in the above mentioned studies also differs.

Motivated by the success of ICA based CI artifacts attenuation methods for transient responses, an ICA based CI artifacts attenuation method for EASSRs with automated IC selection has been developed in [30], and compared to the LI method in one subject. This study aims to apply and evaluate this method in a larger pool of subjects, and for different stimulation parameters. Three datasets were selected, with overlapping and non-overlapping CI artifacts, and EASSRs of various SNRs. The first dataset contains high SNR EASSRs, elicited by 40 Hz AM 500 pps pulse trains presented at C level, resulting in non-overlapping CI artifacts in contralateral recording channels. The second dataset was acquired in the same subjects, and contains no or low SNR EASSRs, elicited by 90 Hz AM 500 pps pulse trains presented at C level. Again, non-overlapping CI artifacts are present in contralateral recording channels. The last dataset consists of EASSRs with various SNRs, elicited by 40 Hz AM 900 pps pulse trains presented at various stimulation levels. CI artifacts mostly overlap in these measurements. For non-overlapping CI artifacts, the results obtained with the ICA based CI artifacts attenuation method are compared to the results obtained with LI. Given the challenges of using ICA for CI artifacts attenuation in EASSR measurements on the one hand, and the reported success of the method for cortical responses on the other hand, we do not formulate any hypothesis concerning the performance of the method. The aim of this study was to apply the method on several datasets, with a wide variety of CI artifacts and EASSR characteristics, in order to determine whether the method gives acceptable results.

2. Materials and methods

2.1. Datasets

Three datasets, with overlapping and non-overlapping CI artifacts, and containing EASSRs with various SNRs, were used to evaluate the ICA based CI artifacts attenuation method. For all three datasets, all subjects wore Cochlear Nucleus® implants, see table 1.

The first two datasets, with non-overlapping CI artifacts, are adopted from [17], where modulation frequency transfer functions (MFTFs) have been acquired for six adult post-lingually deafened CI subjects in two frequency ranges. In the MFTF datasets, stimulation at $f_c = 500$ pps was used, where LI successfully removes CI artifacts in contralateral recording channels [17]. In the contralateral recording channels, the EASSRs obtained with the ICA method can therefore be compared to the baseline measures obtained with LI.

The third dataset, with overlapping CI artifacts, was collected specifically for this study, where amplitude growth functions (AGFs) have been measured in seven adult post-lingually deafened CI subjects. In the AGF dataset, the clinical pulse rate of $f_c = 900$ pps for Cochlear Nucleus® implants was used, resulting in mostly overlapping CI artifacts. No baseline EASSR measures are thus available for this dataset.

Table 1. Subject details, including reference channel (Ref) and set of channels (c_C and c_I) used for analysis in the contralateral (C) and ipsilateral (I) hemisphere per subject, for MFTF and AGF datasets.

S (R/L)	Type	Ref	C (c_C)	I (c_I)
MFTF				
S01 (R)	CI24RE	C_z	CP_5, P_5, P_7, P_9, PO_3, PO_7, TP_7, O_1	CP_6, PO_4, O_2
S02 (R)	CI24RE	C_z	CP_5, P_5, P_7, P_9, PO_3, PO_7, TP_7, O_1	CP_6, PO_4, O_2
S03 (L)	CI24RE	C_z	CP_6, P_6, P_8, P_{10}, PO_4, PO_8, TP_8, O_2	CP_5, P_5, PO_7, O_1
S04 (R)	CI422	Fp_z	CP_5, P_5, P_7, P_9, PO_3, PO_7, TP_7, O_1	CP_6, PO_4, O_2
S05 (R)	CI24RE	Fp_z	CP_5, P_5, P_7, P_9, PO_3, PO_7, TP_7, O_1	PO_4, O_2
S06 (L)	CI24RE	C_z	CP_6, P_6, P_8, P_{10}, PO_4, PO_8, TP_8, O_2	CP_5, P_5, PO_3, PO_7, O_1
AGF				
S02 (R)	CI24RE	C_z	CP_5, P_5, P_7, P_9, PO_4, PO_7, TP_7, O_1	CP_6, P_{10}, TP_8, O_2
S04 (R)	CI422	C_z	CP_5, P_5, P_7, P_9, PO_4, PO_7, TP_7, O_1	CP_6, P_6, PO_4, PO_8, O_2
S07 (L)	CI24R	C_z	CP_6, P_6, P_8, P_{10}, PO_4, PO_8, TP_8, O_2	CP_5, P_5, P_7, P_9, PO_4, PO_7, TP_7, O_1
S08 (L)	CI24M	C_z	CP_6, P_6, P_8, P_{10}, PO_4, PO_8, TP_8, O_2	CP_5, P_5, PO_3, O_1
S09 (L)	CI24R	C_z	CP_6, P_6, P_8, P_{10}, PO_4, PO_8, TP_8, O_2	CP_5, P_5, PO_3, TP_7, O_1
S10 (L)	CI24RE	C_z	CP_6, P_6, P_8, P_{10}, PO_4, PO_8, TP_8, O_2	CP_5, PO_3, O_1
S11 (L)	CI24R	C_z	CP_6, P_6, P_8, P_{10}, PO_4, PO_8, TP_8, O_2	CP_5, PO_3, O_1

Five minute recordings were made in a soundproof and electrically shielded room. Subjects were seated in a comfortable chair and were asked to move as little as possible. A subtitled movie of their choice was played, to guarantee the same attentional state across measurements.

2.1.1. MFTF datasets. Two parts of the dataset described in [17] were used to evaluate the ICA based CI artifacts attenuation method. EASSRs were recorded for a f_m wide range, between 1 and 100 Hz, during multiple recording sessions. Amplitude modulated (AM) high-rate $f_c = 500$ pps pulse trains were presented in MP mode, between intracochlear electrode 11 and the two extra-cochlear electrodes (MP1+2), at maximum comfort level. T and C levels were determined for stimulation with unmodulated pulse trains (T_u and C_u), as well as the C level for stimulation with AM modulated pulse trains (C_m) with minimal level T_u. The stimuli were AM pulse trains, modulated in amperes between T_u and C_m.

The EEG was recorded with a 64-channel ActiveTwo Biosemi system, with a sampling rate of 8192 Hz and a built-in low pass filter with 1638 Hz cutoff. At the start of each 1.024 s epoch, triggers were sent to the recording system.

EASSRs were prominently present in all subjects, for f_m between 30 and 50 Hz [17]. Significant 80–100 Hz f_m EASSRs could only be detected in a limited number of measurements: this could possibly be caused by the long period of auditory deprivation in these subjects. More details can be found in [17].

Here, per subject, seven recordings with f_m between 30 and 51 Hz with high SNR EASSRs (further called 40 Hz MFTF dataset), and eight recordings with f_m between 80 and 100 Hz with absent or low SNR EASSRs (further called 90 Hz MFTF dataset), were used for the evaluation of the ICA based CI artifacts attenuation method. In subject S06, only four recordings with f_m between 80 and 100 Hz were acquired due to time constraints during the first recording session.

2.1.2. AGF dataset. With objective CI fitting in mind, EASSR amplitude growth functions (AGFs) were measured with $f_c = 900$ pps MP stimulation. If the CI artifacts can be attenuated successfully, objective T levels can be determined from these data. Again, T and C levels were determined behaviorally for stimulation with unmodulated pulse trains (T_u and C_u). The C level for AM modulated pulse trains with minimal level T_u was determined (C_m). The modulation depth MD was then fixed to $MD = \frac{C_m - T_u}{C_m + T_u}$, and the T level for AM modulated pulse trains was determined (T_m). The stimuli were 37 Hz and 42 Hz AM pulse trains with fixed modulation depth MD at different stimulation levels, ranging from below T_m to C_m. Stimulation levels were selected per subject, according to the testing time. In the following, stimulation levels SL are expressed in % dynamic range (%DR), defined as $100\ \frac{SL - T_m}{C_m - T_m}$. Hence, 0%DR corresponds to stimulation at T_m. Recordings were obtained with the same recording system as in [17], described in section 2.1.1.

2.2. Signal processing

The raw signals $x[t, c]$, with t the time index and c the recording channel index, were stored in a matrix $\in \mathbb{R}^{N_t \times N_c}$, with N_t and N_c the number of time samples and channels, respectively.

Two recording channel sets were defined for analysis: (1) $c_L = \{CP_5, P_5, P_7, P_9, PO_4, PO_7, TP_7, \text{and } O_1\}$ in the left hemisphere, and (2) $c_R = \{CP_6, P_6, P_8, P_{10}, PO_4, PO_8, TP_8, \text{and } O_2\}$ in the right hemisphere. As in [17, 29], channels located on top of the CI, and channels with excessive noise levels, were excluded from the analysis. The set of channels used is detailed in table 1. Subjects S02 and S04 were included in the MFTF datasets, as well as the AGF dataset. The channel sets used for analysis of the datasets differ, due to different placement of the electrode cap in recording sessions taking place on different dates. Three different signal processing methods were assessed: (1) no CI artifacts attenuation (NO); (2) linear interpolation (LI); (3) ICA based CI artifacts attenuation (ICA). Note that most recording channels were included for the ICA decomposition, see also section 2.2.3, and that the channels sets in table 1 are merely used for analysis.

The first two processing methods are very similar to the methods described in [29].

2.2.1. No CI artifacts attenuation (NO). To remove DC bias, raw signals $x[t, c]$ were high pass filtered with a zero-phase second order Butterworth filter with 2 Hz cutoff frequency. The filtered signals were then split in 1.024 s epochs based on the trigger signal at the start of each epoch, and 5% of the epochs were rejected based on their peak-to-peak amplitude to eliminate excessive movement, ocular, and muscle artifacts. The epoch signals were stored in a three-dimensional tensor $\mathcal{X}_{\mathrm{NO}}[t', e, c] \in \mathbb{R}^{N_{t'} \times N_e \times N_c}$, with $N_{t'}$ the number of time samples in one epoch and N_e the number of epochs. The Fourier transform $\overline{\mathcal{X}}_{\mathrm{NO}}[f, e, c]$ of the epoch signals was then determined for each epoch $e = 1 \ldots N_e$ and channel $c = 1 \ldots N_c$. These signals were rereferenced to either C_z or Fp_z, as indicated in table 1, by subtracting this reference signal, resulting in the tensor $\overline{\mathcal{X}}^{r}_{\mathrm{NO}}[f, e, c]$.

The average signals $\overline{\mathcal{X}}^{r,C}_{\mathrm{NO}}[f, e]$ and $\overline{\mathcal{X}}^{r,I}_{\mathrm{NO}}[f, e]$ were determined as the mean over the selected channels c_C and c_I in the contralateral and ipsilateral hemisphere.

$$\overline{\mathcal{X}}^{r,C}_{\mathrm{NO}}[f, e] = \mathrm{mean}(\overline{\mathcal{X}}^{r}_{\mathrm{NO}}[f, e, c])_{c_C} \tag{1}$$

$$\overline{\mathcal{X}}^{r,I}_{\mathrm{NO}}[f, e] = \mathrm{mean}(\overline{\mathcal{X}}^{r}_{\mathrm{NO}}[f, e, c])_{c_I}. \tag{2}$$

The synchronous activity $\overline{m}^{r,C/I}_{\mathrm{NO}}$, consisting of EASSR and CI artifacts, was calculated as the component at f_m, averaged over epochs.

$$\overline{m}^{r,C/I}_{\mathrm{NO}} = \mathrm{mean}(\overline{\mathcal{X}}^{r,C/I}_{\mathrm{NO}}[f_m, e])_e. \tag{3}$$

The synchronous amplitude and phase were determined as the absolute value and angle of the synchronous activity.

$$\begin{aligned} A^{r,C/I}_{\mathrm{NO}} &= |\overline{m}^{r,C/I}_{\mathrm{NO}}| \\ \theta^{r,C/I}_{\mathrm{NO}} &= \angle \overline{m}^{r,C/I}_{\mathrm{NO}}. \end{aligned} \tag{4}$$

The non-synchronous activity is the standard deviation of the component at f_m over epochs, divided by the square root of the number of epochs N_e.

$$N^{r,C/I}_{\mathrm{NO}} = \frac{\mathrm{std}(\overline{\mathcal{X}}^{r,C/I}_{\mathrm{NO}}[f_m, e])_e}{\sqrt{N_e}}. \tag{5}$$

The Hotelling T^2 test [19] compares the real and imaginary components of the synchronous activity to the non-synchronous activity to determine whether significant synchronous activity, relative to the neural background noise, is present. $A^{r,C/I}_{\mathrm{NO}}$ and $\theta^{r,C/I}_{\mathrm{NO}}$ are used further on to compare the three methods.

2.2.2. Linear interpolation (LI). A linear interpolation, with duration $d = t_{\mathrm{post}} - t_{\mathrm{pre}}$, was applied for each stimulation pulse between a pre-stimulus sample t_{pre} and a post-stimulus sample t_{post} that are both assumed to be free from CI artifacts.

The maximum value for d is the interpulse interval, i.e. the inverse of the pulse rate, in this case 2 ms for $f_c = 500$ pps, and 1.1 ms for $f_c = 900$ pps. In that case, only one sample per stimulation pulse is retained, and the remaining samples are interpolated. In accordance to previous studies [17, 29], the pre-stimulus sample was always chosen at 0.1 ms before the start of the stimulation pulse, the post-stimulus sample was chosen at either 1.9 ms for $f_c = 500$ pps or 1 ms for $f_c = 900$ pps, after the start of the stimulation pulse. Further processing followed the steps outlined above in section 2.2.1, i.e. high pass filtering, transformation to frequency domain, averaging over channels and epochs with (1, 2, 3), synchronous ($A^{r,C/I}_{\mathrm{LI}}$ and $\theta^{r,C/I}_{\mathrm{LI}}$, with (4)) and non-synchronous activity ($N^{r,C/I}_{\mathrm{LI}}$, with (5)) calculation, and testing for significant synchronous activity with the Hotelling T^2 test. It has been shown in [17, 24] that LI sufficiently attenuates CI artifacts in contralateral recording channels for $f_c = 500$ pps.

2.2.3. ICA based CI artifacts attenuation (ICA). Channels located on top of the CI coil were removed prior to ICA decomposition. All remaining channels were included for the ICA decomposition, and the channel sets described in table 1 were used for analysis. The raw signals $x[t, c]$ were filtered with a second-order 2 Hz high-pass filter to remove any DC bias. Next, the signals were split into epochs of 1.024 s, based on the trigger signal, and 5% of the epochs were rejected to eliminate excessive movement, ocular and muscle artifacts. The resulting epochs were concatenated and transposed into $X = x[c, \tilde{t}]$, and then used as the input to the Infomax ICA algorithm as implemented in EEGLAB (v 11.0.5.4b) [40] with default settings. The Infomax ICA implementation was used, because it has widely and successfully been applied to EEG data [14, 15, 33, 41–43]. The ICA algorithm determines the unmixing matrix W such that independent component (ICs) S are obtained from X:

$$S = W\,X \tag{6}$$

$$X = P\,S. \tag{7}$$

The mixing matrix $P = W^{-1}$ describes how the ICs are mixed together to reconstruct X. ICA aims to separate the EEG signals into statistically maximally independent ICs. Contrary to the methods used in the above mentioned studies, here, no band pass filtering or down-sampling was applied to the data in order to preserve the f_c component, that is used for automated artifactual IC selection.

ICs corresponding to CI artifacts are normally selected manually based on temporal and topographic characteristics. Manual IC selection is a subjective and time-consuming process. Hence, a heuristic approach to automatically select ICs corresponding to CI artifacts was used. It is assumed that ICs contain either EASSR, CI artifacts, ocular, or muscle artifacts, or neural background noise. Only CI artifacts have high frequency components above 200 Hz. Artifactual ICs can therefore be identified based on the spectral amplitude at f_c [30]. It is not possible to directly identify artifactual ICs based on the spectral amplitude at f_m, because ICs with a significant f_m component may represent either CI artifacts, or a genuine ASSR.

Each IC was reconstructed in channel space, by multiplying the time course of the IC (ith row of S for IC_i) by its spatial distribution (ith column of P for IC_i). All ICs with a CI

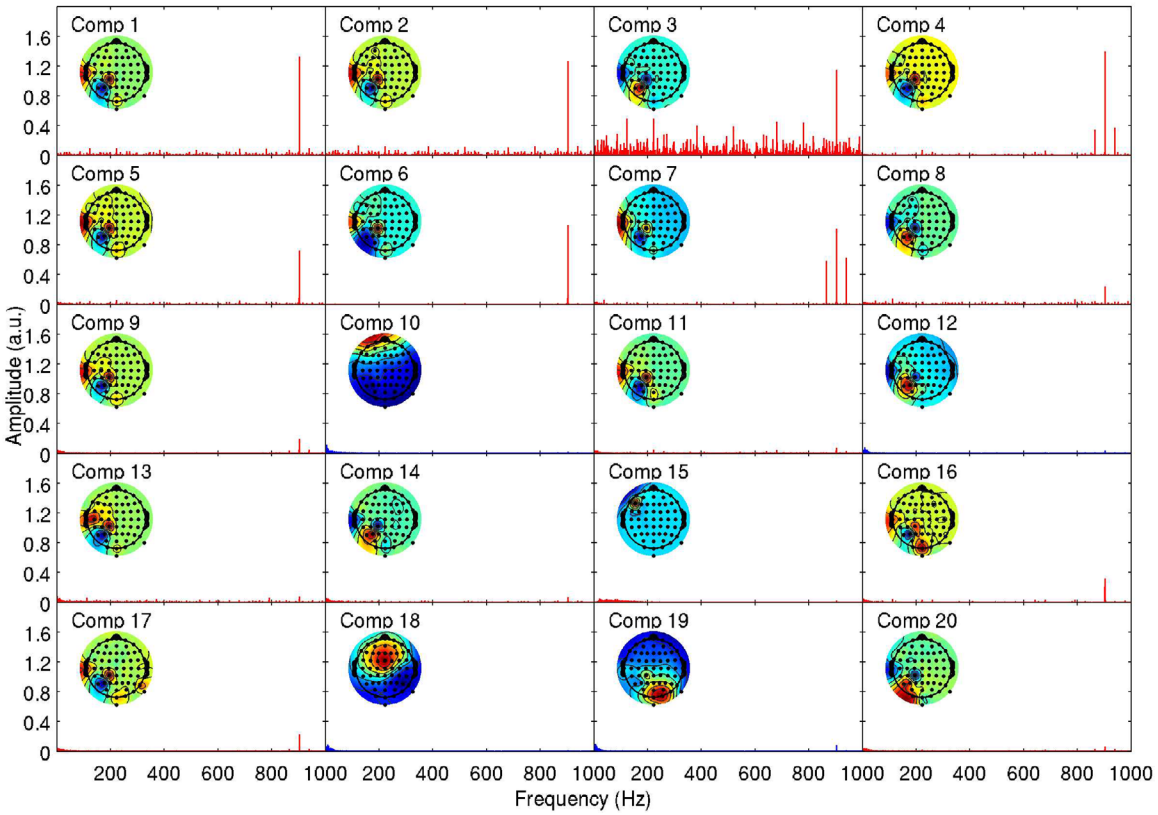


Figure 2. First 20 ICs obtained after ICA for subject S07, recording 1 (AGF dataset). For each IC, the amplitude spectrum, and the spatial distribution over recording channels is shown. The amplitude spectrum is colored red for rejected ICs, and blue for the remaining ICs.

artifacts contribution at f_m in any recording channel higher than the noise level were identified as CI artifacts ICs. Two assumptions are made for the CI artifacts IC spectra; (1) the spectral amplitude at the sidebands $f_c \pm f_m$ is related to the spectral amplitude at f_c through the modulation depth MD: $A_{f_c \pm f_m} = \frac{MD}{2} A_{f_c}$, which is valid for an ideal AM signal, and (2) the spectral amplitude at f_m is equal to the spectral amplitude at the sidebands: $A_{f_m} = A_{f_c \pm f_m}$. With these assumptions, we have $A_{f_c} = \frac{2}{MD} A_{f_m}$. A threshold t_i was defined for each IC_i such that if its spectral amplitude A_{IC_i,f_c} at f_c in source space, was smaller than the threshold, then the spectral amplitude A_{IC_i,c,f_m} at f_m in channel c after reconstruction, was smaller than the noise level, N_{f_m}. Mathematically: if $A_{\mathrm{IC}_i f_c} \leqslant \mathrm{t_i}$, then $A_{\mathrm{IC}_i,c,f_m} \leqslant N_{f_m}$. As the conversion from source space to channel space for IC_i is determined by the ith column P_i of the mixing matrix P, the largest contribution of IC_i to any channel is thus given by the largest element of P_i ($\max_{P_i}$). The resulting threshold t_i for IC_i is then equal to $\frac{2}{MD \ \max_{P_i}} N_{f_m}$.

In reality, the CI artifacts are not ideal AM signals and the spectral amplitude at f_m depends on the non-linearity of the CI artifacts propagation. The noise levels used were 25 nV for the responses in the 40 Hz range, and 5 nV for the responses in the 90 Hz range, which are the expected N_{f_m} values, for 5 min recordings [4]. Alternatively, noise levels can be determined for each subject separately.

Because the spectral amplitude at f_c is compared to the threshold, and assuming the ICA decomposition is successful such that each IC contains either EASSR or CI artifacts, it is ensured that only the CI artifacts are attenuated and that the EASSR itself is unchanged. If the ICA decomposition is not successful, ICs may contain both CI artifacts and EASSR, and rejection of these ICs may lead to attenuation of the EASSR.

The CI artifacts ICs were identified as described above, and rejected, and the remaining ICs were projected back to the original recording channels, using the mixing matrix P. Further processing followed the steps outlined above in section 2.2.1, i.e. transformation to frequency domain, reference channel subtraction, averaging over channels and epochs (with (1, 2, 3), synchronous ($A^{r,C/I}_{\mathrm{ICA}}$ and $\theta^{r,C/I}_{\mathrm{ICA}}$, with (4)) and non-synchronous activity ($N^{r,C/I}_{\mathrm{ICA}}$, with (5)) calculation, and testing for significant synchronous activity with the Hotelling T^2 test.

2.3. Evaluation

2.3.1. Response properties after ICA based CI artifacts attenuation. Evaluating the quality of the CI artifacts attenuation is difficult as there generally is no golden standard available. However, it has recently been shown that it is possible to obtain reliable EASSRs in contralateral recording channels with stimulation at 500 pps and LI [17, 24]. Therefore, for the *MFTF* datasets, with $f_c = 500$ pps, EASSR amplitudes $A^{r,C}$ and phases $\theta^{r,C}$ should be similar with LI and ICA based CI artifacts attenuation.

As in [17, 29], response latencies were determined. The slope of the $\theta(f_m)$ curve, which is related to the neural response latency, indicates whether the measurement is EASSR or CI artifacts dominated. For significant EASSRs, the EASSR phase $\theta(f_m)$ should decrease linearly with increasing

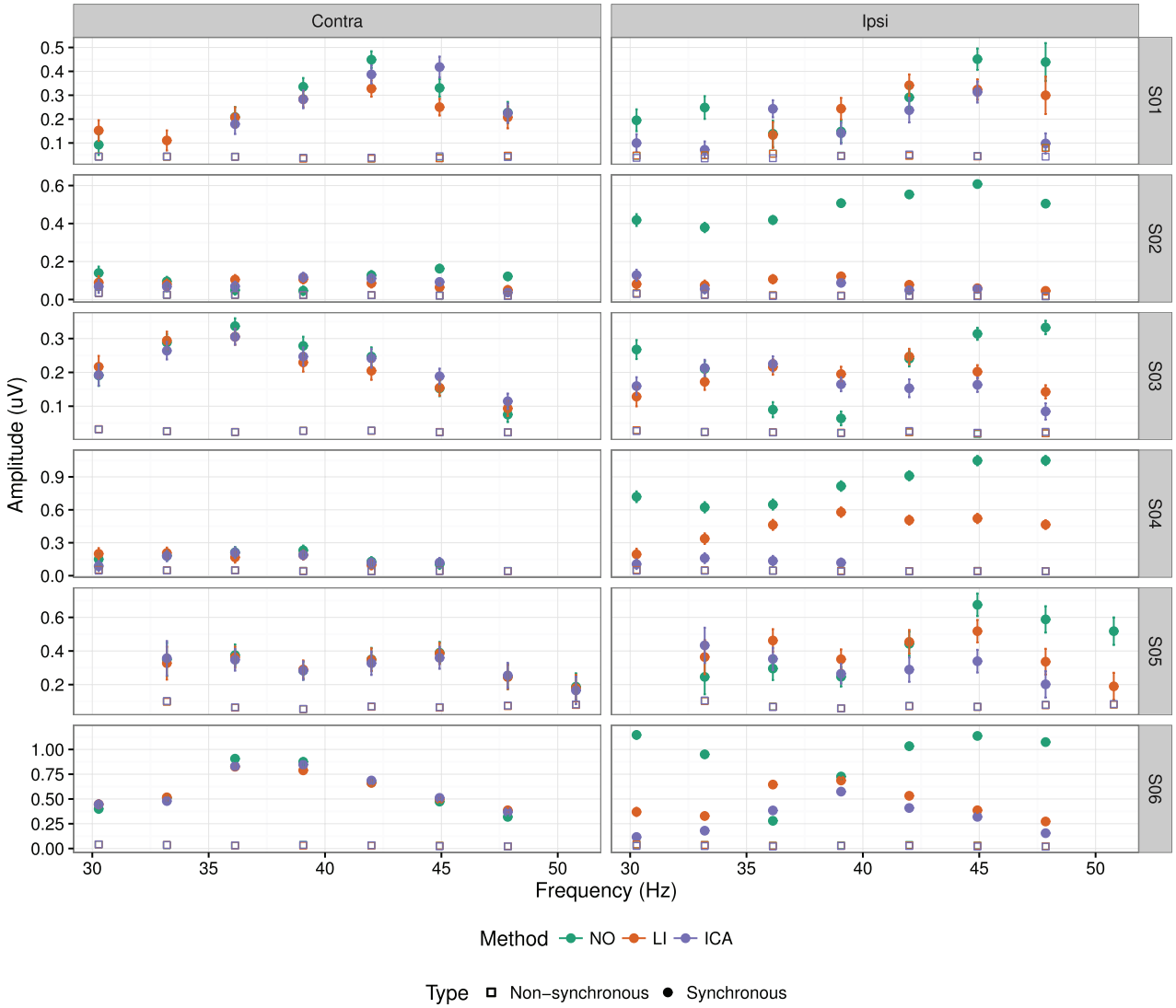


Figure 3. 40 Hz MFTF dataset: $A^{r,C/I}$ (◦) and $N^{r,C/I}$ (□) for NO, LI and ICA for the mean contra- and ipsilateral recording channel and for subjects S01-S06. Error bars represent the noise level $N^{r,C/I}$. Only EASSR or CI artifacts dominated data points are included.

modulation frequency f_m in the 30–50 Hz range and in the 80–100 Hz range [17, 18]. Response phases are stable at multiples of 180 degrees, independent of the modulation frequency, when measurements are CI artifacts dominated [4, 5, 17]. The response latency L was calculated as the additive inverse of the slope of the $\theta(f_m)$ curve, for the mean contra- and ipsilateral channel. For the 40 Hz MFTF dataset, response latencies were also determined for the individual channels in the selected sets.

In [17], the response latency was determined for all contralateral recording channels, and the median (44.2 ms) and interquartile range (6.8 ms) over the selected channels are used as a reference value in this study. Note that the response latency calculation is different in this study: L is determined for the EEG signal averaged over the channel selection, instead of taking the median of L calculated for separate channels.

For the *AGF dataset*, with $f_c = 900$ pps, no ground truth is available. However, from EEG signals recorded in normal-hearing subjects and in CI subjects with BP stimulation, there is some knowledge available about the properties of the EASSR. EASSR amplitudes generally grow nonlinearly with increasing stimulation levels, and range between 0 to 1000 nV [4, 17, 18, 44]. No EASSR should be detected below the subjects' behavioral threshold. The EASSR phase difference, measured between two different modulation frequencies, should be stable when an EASSR is present and depends on the modulation frequency difference [4]. The response latency L can be computed from the two response phases $\theta(f_{m1})$ and $\theta(f_{m2})$ for the two modulation frequencies $f_{m1} = 37$ and $f_{m2} = 42$ Hz.

$$L = \frac{\theta(f_{m2}) - \theta(f_{m1})}{360°(f_{m1} - f_{m2})}. \tag{8}$$

2.3.2. Noise level reduction and number of rejected ICs. The ICA decomposition aims to separate EASSR, CI artifacts, ocular and muscle artifacts, and neural background noise. In case of perfect separation, the neural background noise level and EASSR amplitude should not be attenuated when the CI artifacts ICs are rejected. For the 40 Hz AGF dataset, there

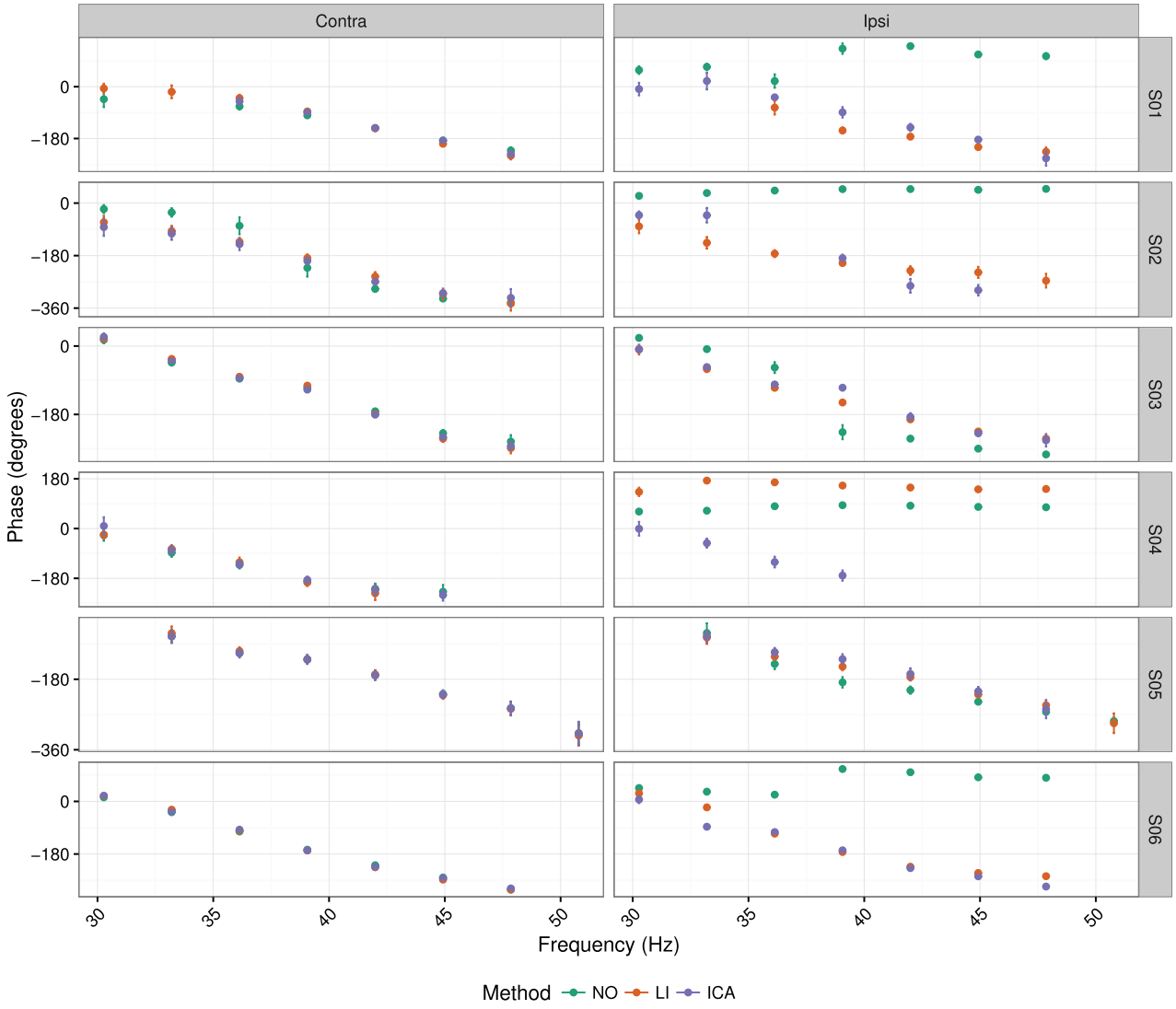


Figure 4. 40 Hz MFTF dataset: $\theta^{r,C/I}$ for NO, LI and ICA for the mean contra- and ipsilateral recording channel and for subjects S01-S06. Only EASSR or CI artifacts dominated data points are included.

are no baseline values available for the EASSR amplitude, but the change in neural background noise level can be used. Neural background noise levels N_{ICA} that deviate much from the initial values obtained without CI artifacts rejection N_{NO} indicate that the ICA does not completely separate CI artifacts and neural background noise.

The reduction in neural background noise levels was therefore calculated from the non-synchronous activity computed with (5) in sections 2.2.1–2.2.3, as follows:

$$\Delta N_{\mathrm{LI-NO}} = \frac{N_{\mathrm{LI}}^{r,C/I}[f_m] - N_{\mathrm{NO}}^{r,C/I}[f_m]}{N_{\mathrm{NO}}^{r,C/I}[f_m]} \tag{9}$$

$$\Delta N_{\mathrm{ICA-NO}} = \frac{N_{\mathrm{ICA}}^{r,C/I}[f_m] - N_{\mathrm{NO}}^{r,C/I}[f_m]}{N_{\mathrm{NO}}^{r,C/I}[f_m]}. \tag{10}$$

For each recording, the number of rejected ICs was determined. First, the number of ICs explaining 99% of the raw signals' variance ($\#_{\mathrm{IC}_{99}}$) was computed. Second, within the set of ICs explaining 99% of the variance, the number of rejected ICs ($\#_{\mathrm{IC}_{\mathrm{rej}}}$) and the variance explained by these ICs ($\mathrm{var}_{\mathrm{IC}_{\mathrm{rej}}}$) was determined. For each subject, the mean value and range of $\#_{\mathrm{IC}_{\mathrm{rej}}}$ and $\mathrm{var}_{\mathrm{IC}_{\mathrm{rej}}}$ were determined over all recordings in this subject. For a perfect ICA decomposition, it is expected that the CI artifacts are expressed only on a small number of ICs. Therefore, a large number of rejected ICs indicates that the ICA decomposition is unsuccessful in completely separating CI artifacts and EASSR.

3. Results

Figure 2 shows the first 20 ICs obtained after ICA decomposition for the first recording in the AGF dataset of subject S07. The amplitude spectrum up to 1000 Hz is plotted, and the scalp plot shows the spatial distribution of the IC over the recording channels. The scalp projections were normalized, for illustration purposes, but scalp projections are usually larger for the first ICs. Rejected ICs have a clear peak at f_c, and show a centroid at the side of the CI (left for subject S07). In some rejected ICs, the sidebands, caused by the modulation of the

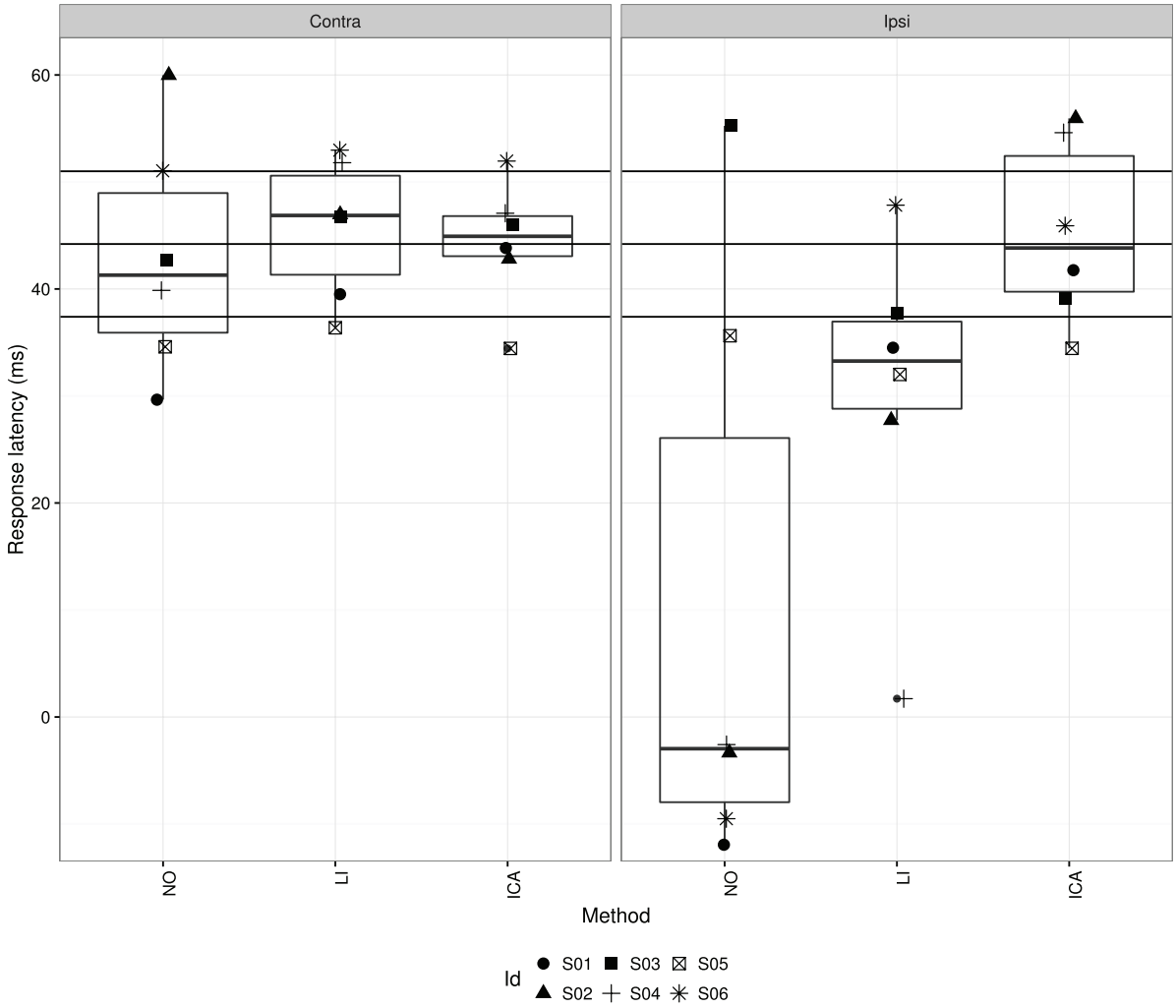


Figure 5. 40 Hz MFTF dataset: response latency for NO, LI and ICA for the mean contra- and ipsilateral recording channel and for subjects S01-S06. The expected range (median: 44.2 ms, interquartile range: 6.8 ms), obtained from [17], is indicated with horizontal lines.

pulse train, are clearly visible. Neural background noise, with the typical $1/f$ spectrum, is clearly present in some rejected ICs, e.g. IC9.

Two MFTF datasets and one AGF dataset were used: (1) 40 Hz MFTF, (2) 90 Hz MFTF, and (3) 40 Hz AGF. The results are discussed in detail below.

3.1. 40 Hz MFTF dataset

Figure 3 contains $A_{\mathrm{NO}}^{r,C/I}$, $A_{\mathrm{LI}}^{r,C/I}$, and $A_{\mathrm{ICA}}^{r,C/I}$ for the mean contra- and ipsilateral recording channel. In the mean contralateral channel (left panel), amplitudes are similar for all three methods and error bars overlap for LI and ICA, indicating that LI and ICA lead to similar results, and ICA is not distorting the EASSR. In the mean ipsilateral channel (right panel), LI cannot remove all CI artifacts for all subjects [17, 24]: $A_{\mathrm{LI}}^{r,I}$ can therefore not be seen as the baseline truth. $A_{\mathrm{ICA}}^{r,I}$ is mostly smaller than $A_{\mathrm{LI}}^{r,I}$, especially in the higher frequencies (>40 Hz), suggesting that ICA is better capable than LI of attenuating CI artifacts in the ipsilateral hemisphere.

The same observations can be made based on the synchronous phase $\theta_{\mathrm{NO}}^{r,C/I}$, $\theta_{\mathrm{LI}}^{r,C/I}$, and $\theta_{\mathrm{ICA}}^{r,C/I}$, given in figure 4, and the response latencies $L_{\mathrm{NO}}^{r,C/I}$, $L_{\mathrm{LI}}^{r,C/I}$, and $L_{\mathrm{ICA}}^{r,C/I}$, given in figure 5. In the mean contralateral channel (left panels), phases decrease linearly with increasing f_m for all methods, indicating that the measurements are EASSR dominated, even before CI artifacts attenuation, and that all methods lead to similar results. Response latencies $L_{\mathrm{NO}}^{r,C}$, $L_{\mathrm{LI}}^{r,C}$, and $L_{\mathrm{ICA}}^{r,C}$, are also similar and within the expected range obtained in [17]. In the ipsilateral hemisphere (right panels), $\theta_{\mathrm{NO}}^{r,I}$ is constant for increasing f_m, resulting in small $L_{\mathrm{NO}}^{r,I}$, for subjects S01, S02, S04 and S06. This confirms that the measurements are indeed CI artifacts dominated in the ipsilateral hemisphere. $\theta_{\mathrm{LI}}^{r,I}$ is still constant for increasing f_m for subjects S02, and S04, confirming that LI is indeed incapable of removing all CI artifacts in the ipsilateral hemisphere for all subjects. With ICA, $\theta_{\mathrm{ICA}}^{r,I}$ linearly decreases with increasing f_m for all subjects, and the obtained response latencies are close to the expected values for all subjects. As noted before, L is calculated differently in this study than in [17]; the obtained values are therefore slightly different from the used reference values.

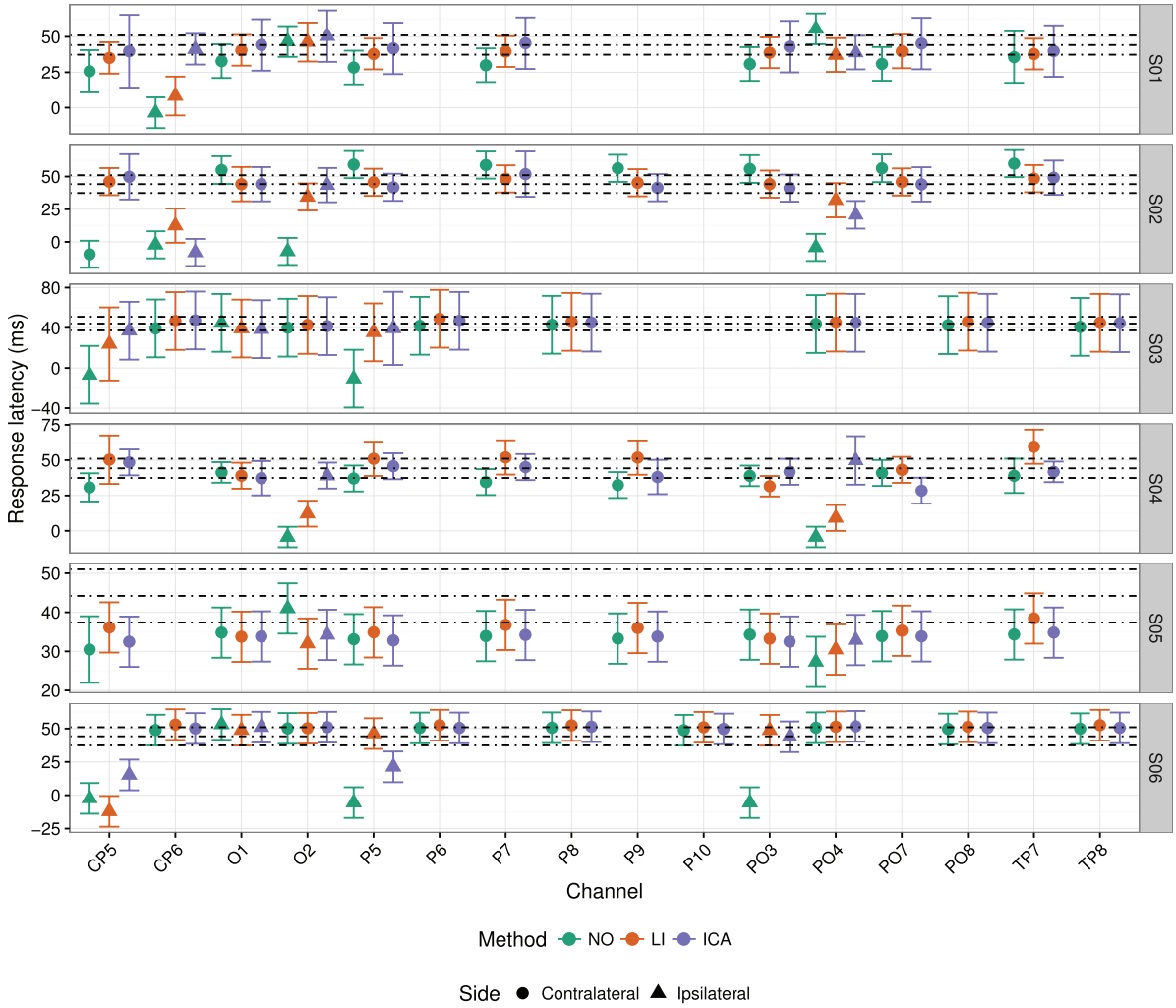


Figure 6. 40 Hz MFTF dataset: response latencies in individual channels for NO, LI and ICA and for subjects S01-S06.

Good results are thus obtained for mean contra- and ipsilateral channels. Response latencies in individual recording channels are given in figure 6. Overall, response latencies are mostly within the expected range for all three methods. However, some clear improvements of ICA compared to either NO or LI can be seen, i.e. channel CP_6 for S01, channels CP_5, O_2 and PO_4 for S02, channel O_2 and PO_4 for S04, and channel PO_3 for S06. In some cases, ICA performs similarly bad as LI, i.e. channels CP_6 in S02, and channel CP_5 in S06. ICA performs worse than LI, in channel P_5 in S06.

3.2. 90 Hz MFTF dataset

No consistent 90 Hz EASSRs have been found in the contralateral channels in [17]. In figure 7, it is shown that synchronous amplitudes are largely attenuated by LI and ICA, compared to NO. However, in all subjects but S05, significant synchronous activity was still detected in some data points after ICA. Based on the synchronous phases, it cannot be concluded that these data points are not CI artifacts dominated, and too few data points are available to evaluate the EASSR/CI artifacts properties adequately. No conclusions on how ICA preserves or distorts the EASSR can therefore be drawn based on these low SNR recordings.

3.3. 40 Hz AGF dataset

Figure 8(a) shows $A_{\mathrm{LI}}^{r,C/I}$, for varying stimulation levels and $f_m = 37$ and $f_m = 42$ Hz. In general, after LI, $A^{r,C/I}$ is large and increasing linearly with increasing stimulation level. With LI, synchronous components are significantly different from the neural background noise in most data points, including subthreshold stimulation levels. This suggests that measurements are CI artifacts dominated in the contralateral and ipsilateral hemisphere, for all subjects, except S07 and S08. Figure 8(b) shows that $A_{\mathrm{ICA}}^{r,C}$ and $A_{\mathrm{ICA}}^{r,I}$ are similar in order of magnitude. It is clear that $A_{\mathrm{ICA}}^{r,C/I}$ is smaller than $A_{\mathrm{LI}}^{r,C/I}$. For subjects S02, S04, S09, S10 and S11, $A_{\mathrm{ICA}}^{r,C/I}$ changes non-monotonously with increasing stimulation level. In many suprathreshold measurements, no significant synchronous activity is detected, while it is detected in some subthreshold measurements. It seems that ICA attenuates both the CI artifacts, and the EASSR below the noise level in some cases, while in other cases, ICA is

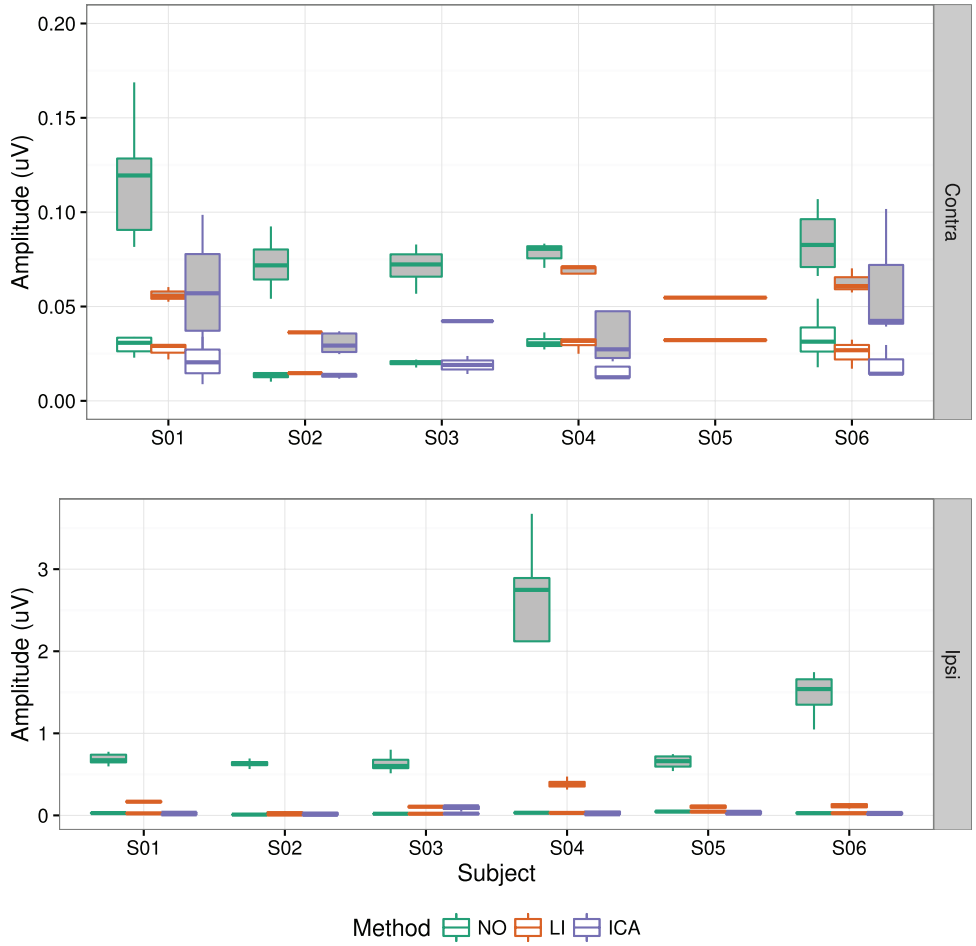


Figure 7. 90 Hz MFTF dataset: $A^{r,C/I}$ (gray fill) and $N^{r,C/I}$ (no fill) for NO, LI and ICA. Only EASSR or CI artifacts dominated data points are included.

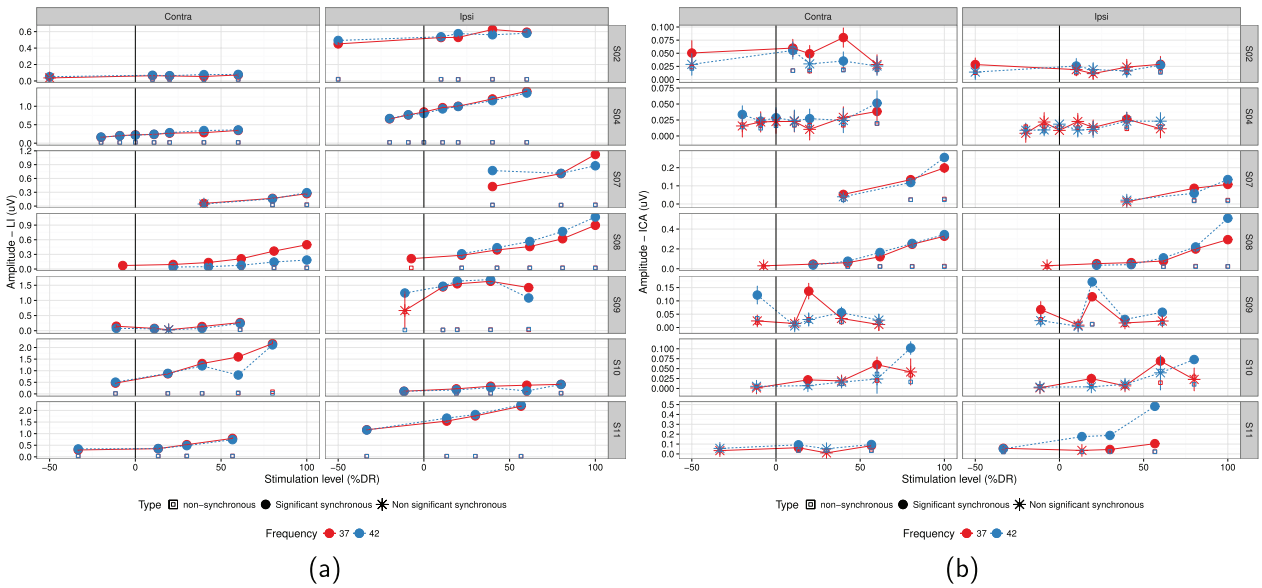


Figure 8. 40 Hz AGF: $A^{r,C/I}$ and $N^{r,C/I}$ for LI (a) and ICA (b), for subjects S02, S04, S07, S08, S09, S10, S11. The vertical lines correspond to the behavioral threshold. (a) LI. (b) ICA.

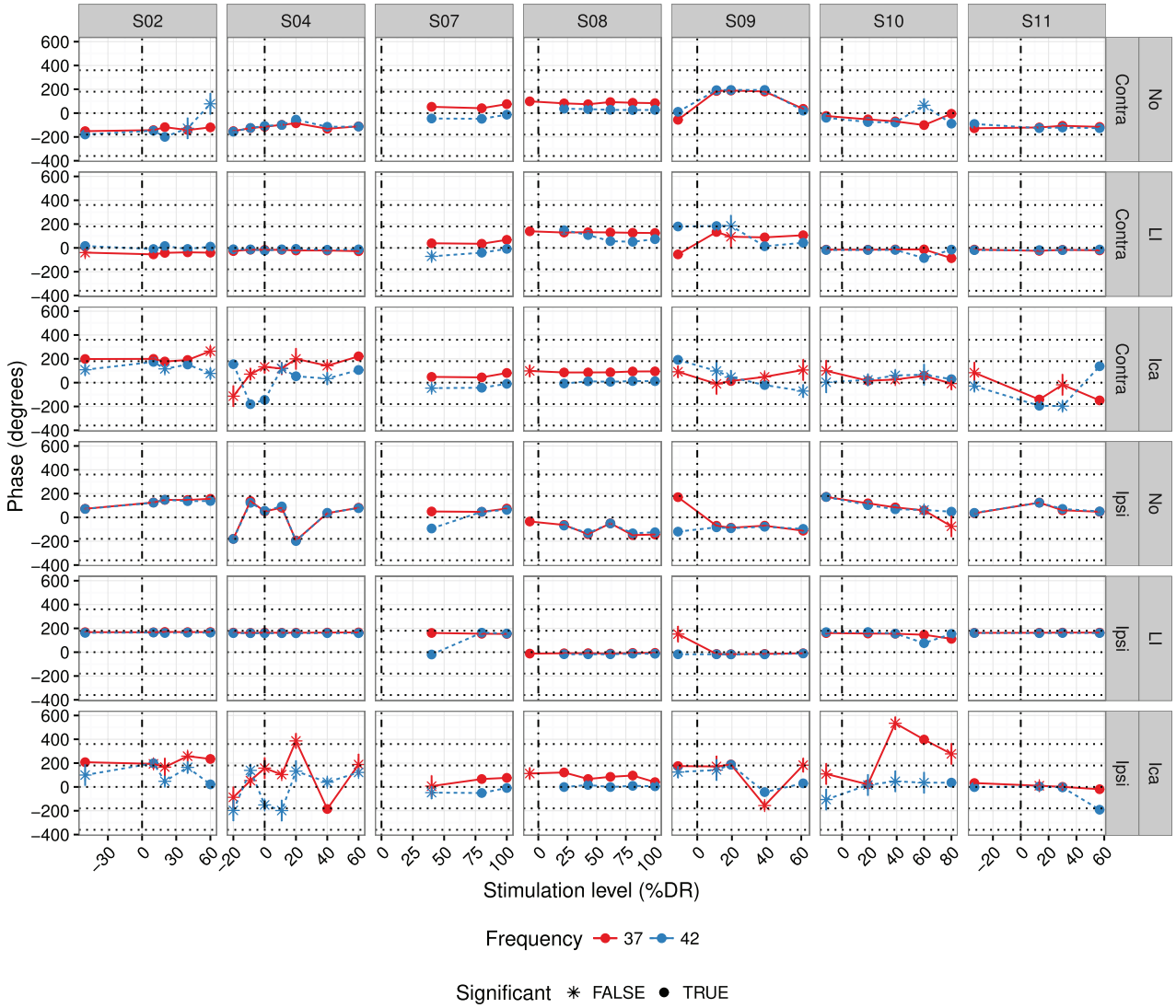


Figure 9. 40 Hz AGF dataset: $\theta^{r,C/I}$ for NO, LI and ICA, for subjects S02, S04, S07, S08, S09, S10 and S11. The vertical lines correspond to the behavioral threshold.

incapable of removing all CI artifacts. For subjects S07 and S08, $A^{r,C/I}_{\mathrm{ICA}}$ does grow nonlinearly and monotonously with increasing stimulation level. Furthermore, significant synchronous activity is detected in most suprathreshold measurements. No synchronous activity is detected at subthreshold stimulation levels for S08. These results suggest that, for S07 and S08, ICA is capable of removing the CI artifacts from contra- and ipsilateral recording channels without distorting the EASSR.

Figure 9 shows $\theta^{r,C/I}_{\mathrm{NO}}$, $\theta^{r,C/I}_{\mathrm{LI}}$ and $\theta^{r,C/I}_{\mathrm{ICA}}$. It is clear that $\theta^{r,C/I}_{\mathrm{NO}}$ and $\theta^{r,C/I}_{\mathrm{LI}}$ are equal for $f_m = 37$ Hz and $f_m = 42$ Hz, and constant over stimulation levels, in both hemispheres for all subjects, except S07 and S08. This confirms that measurements are indeed CI artifacts dominated for NO and LI in the contralateral and the ipsilateral hemisphere, for subjects S02, S04, S09, S10, and S11. In the contralateral hemisphere, in subjects S07 and S08, $\theta^{r,C}_{\mathrm{NO}}$ and $\theta^{r,C}_{\mathrm{LI}}$ are different for $f_m = 37$ Hz and $f_m = 42$ Hz, and constant over stimulation levels. This indicates that measurements are EASSR dominated in the contralateral hemisphere in S07 and S08, for NO and LI.

ICA results in phases $\theta^{r,C/I}_{\mathrm{ICA}}$ that are different for $f_m = 37$ Hz and $f_m = 42$ Hz. However, for most subjects, except S07 and S08, $\theta^{r,C/I}_{\mathrm{ICA}}$ is not stable over stimulation levels. This indicates that ICA is indeed removing CI artifacts from the measurements, but the EASSR is possibly distorted. For S07 and S08, $\theta^{r,C/I}_{\mathrm{ICA}}$ is different for $f_m = 37$ Hz and $f_m = 42$ Hz, and stable over stimulation levels. The phase difference results in a response latency (averaged over hemispheres and stimulation levels resulting in significant EASSRs) of 44 and 49 ms in S07 and S08, respectively. These results confirm that ICA is indeed capable of removing CI artifacts from contralateral and ipsilateral recording channels in S07 and S08.

3.4. Noise level reduction and number of rejected ICs

The noise level reduction, calculated with (10), is shown in figure 10 for the three datasets. Positive values indicate that the noise level is larger after ICA than for NO; negative values indicate smaller noise levels. In the case of perfect ICA separation, no neural background noise would be rejected with the

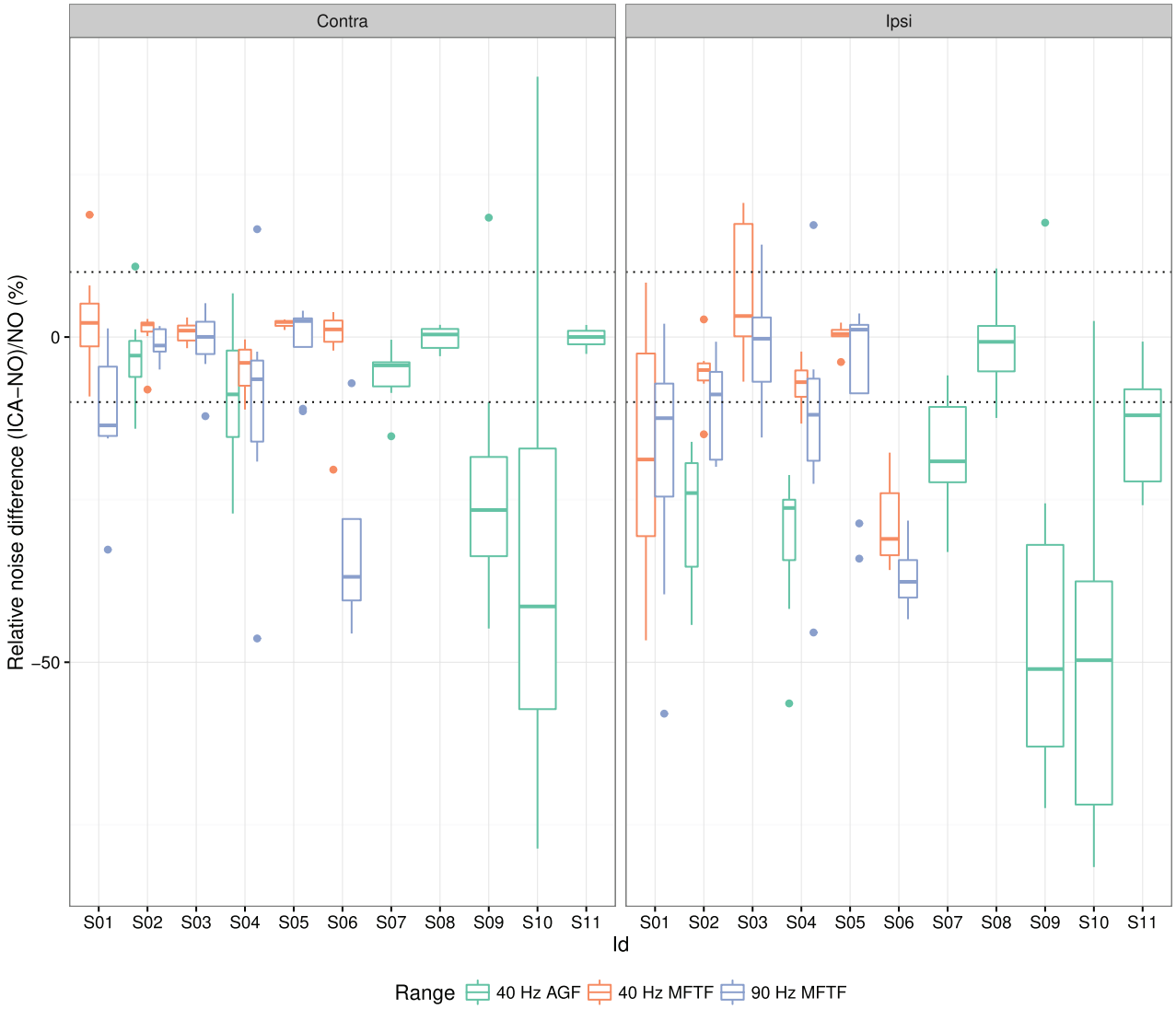


Figure 10. Noise level reduction. Horizontal lines are the 10 and 90 % percentiles of noise reduction levels $\Delta N_{\mathrm{LI-NO}}$ observed with LI compared to NO. In general, noise levels are reduced after ICA, especially at the ipsilateral side. In many cases, $|\Delta N_{\mathrm{ICA-NO}}|$ is larger than $|\Delta N_{\mathrm{LI-NO}}|$. The colored dots represent outliers, i.e. observations that fall outside of the interval $[Q_1 - 1.5\mathrm{IQR}, Q_3 + 1.5\mathrm{IQR}]$, with interquartile range IQR, and the first and third quantile Q_1 and Q_3, respectively.

CI artifacts ICs and hence the noise level would be the same for both methods. Even with LI, a change in the noise levels is observed ($\Delta N_{\mathrm{LI-NO}}$). The 10 and 90 % percentiles of $\Delta N_{\mathrm{LI-NO}}$ were −10 to 10 %, for the three datasets, and are indicated in figure 10 as dashed horizontal lines. With ICA, noise levels change: differences compared to NO of up to 75% are seen, indicating that the ICA separation is definitely not perfect.

For the three datasets, the number of ICs explaining 99% of the raw signals' variance, the number of rejected artifactual ICs and the variance explained by the artifactual ICs are included for each subject in table 2. The number of rejected ICs varies between 3 and 35, with a large amount of explained variance between 80 and 99%, when the outlier of 11% explained variance is discarded. For the AGF dataset, the number of rejected ICs was not significantly different for subthreshold recordings, compared to suprathreshold recordings.

4. Discussion

ICA is often used to remove biological (e.g. ocular, muscle) [40, 41, 43, 45] and CI artifacts [13–15, 31–39] from EEG recordings. This study aims to evaluate the performance of ICA based CI artifacts attenuation on an EEG dataset, containing EASSRs. Three datasets have been used for evaluation, containing either non-overlapping or overlapping CI artifacts in contralateral recording channels, and absent, low SNR, or high SNR EASSRs.

In summary, ICA performs well for all subjects in the 40 Hz MFTF dataset, with high SNR EASSRs and non-overlapping CI artifacts in contralateral recording channels. CI artifacts are greatly attenuated in the 90 Hz dataset, with non-overlapping CI artifacts in contralateral recording channels, and absent or low SNR EASSRs. However, it is unclear whether

the remaining synchronous activity is CI artifacts, or EASSR dominated. In the 40 Hz AGF dataset, with overlapping CI artifacts, and EASSRs with various SNRs, good performance of ICA is observed in two subjects, while the method fails to produce good results in the remaining five subjects. Contradictory results are thus obtained with the three datasets.

4.1. ICA separation quality

Attenuating CI artifacts seems more challenging for EASSR recordings than for transient responses for three reasons. First, in EASSR recordings, the CI artifacts and EASSR overlap continuously in time. On the contrary, the CI artifacts typically precede the neural response for transient responses, with only a limited overlap in time. Second, in EASSR recordings, due to the modulated and asymmetric CI artifacts, the CI artifacts and EASSR also have overlapping spectra. The EASSR is in fact not expected to have any frequency components that are not also present in the CI artifacts spectrum. Both signals have a component at f_m with different amplitude and phase. Third, EASSRs are typically obtained using direct stimulation with one stimulation channel. In the studies that use ICA to measure transient responses [13–15, 31–36], responses are often obtained using free field stimulation, activating multiple stimulation channels without synchronization between the stimulated sequences and the recording epochs. The electrical stimulation patterns elicited by multiple stimulation channels combine, and possibly interfere destructively. Obviously, channel interference is not present when only one channel is stimulated. Furthermore, in previous studies, due to free field stimulation, stimulation sequences are not identical nor perfectly aligned over recording epochs, resulting in attenuated CI artifacts when epochs are averaged to compute the event-related potential.

Figure 11 shows $\theta_{\mathrm{NO}}^{r,C}$ as a function of f_m (for the MFTF datasets) or stimulation level (for the AGF dataset). It suggests that the spatial separation of CI artifacts and EASSR could influence the performance. For all subjects in the 40 Hz MFTF dataset, and for subjects S07 and S08 in the 40 Hz AGF dataset, recordings are EASSR dominated in the contralateral hemisphere, evidenced by $\theta_{\mathrm{NO}}^{r,C/I}$ that changes with changing f_m. On the contrary, recordings are CI artifacts dominated with constant phases for changing f_m, for all subjects (except S05) in the 90 Hz MFTF dataset and for all subjects (except S07 and S08) in the 40 Hz AGF dataset. Recordings can be CI artifacts dominated due to (1) small or absent EASSRs, or (2) large CI artifacts. EASSRs are small in the 90 Hz range [17], and for subjects S02 and S04 in the 40 Hz range ([17] and 3 with synchronous amplitudes of 100–200 nV at comfort level). CI artifacts are large in subjects S09 and S10, see median and range of $A_{\mathrm{NO}}^{r,C}$ in figure 11. No reference data are available for subject S11, it is therefore unknown whether EASSRs are small or CI artifacts are large in this subject.

It seems that ICA is capable of separating CI artifacts and EASSR in case EEG signals in the contralateral hemisphere are EASSR dominated, since a reference for the EASSR source is then available. In other cases, it seems not possible to separate CI artifacts and EASSR. It was suggested in [15] that non-overlapping stimuli and responses are beneficial for ICA based CI artifacts attenuation. Furthermore, lower response SNR may cause more difficulties in separating EASSR and CI artifacts [15].

Table 2. For three datasets: mean (range) of the number ICs explaining 99% of the signals variance ($\#_{\mathrm{IC}_{99}}$), the number of rejected ICs ($\#_{\mathrm{IC}_{\mathrm{rej}}}$), and the variance explained by the rejected ICs ($\mathrm{var}_{\mathrm{IC}_{\mathrm{rej}}}$), for every subject separately and on average (AVG).

S	$\#_{\mathrm{IC}_{99}}$	$\#_{\mathrm{IC}_{\mathrm{rej}}}$	$\mathrm{var}_{\mathrm{IC}_{\mathrm{rej}}}$
40 Hz MFTF			
S01	39 (30–45)	9 (5–12)	87 (80–91)
S02	17 (12–22)	8 (6–10)	97 (97–98)
S03	22 (17–22)	12 (11–15)	97 (96–98)
S04	37 (35–39)	22 (17–29)	93 (91–96)
S05	19 (13–23)	7 (5–8)	95 (94–96)
S06	13 (9–16)	10 (8–11)	99 (98–99)
AVG	25	11	95
90 Hz MFTF			
S01	28 (26–31)	17 (12–22)	97 (95–98)
S02	22 (16–30)	12 (11–14)	97 (96–98)
S03	19 (13–26)	17 (11–21)	99 (98–99)
S04	29 (8–38)	27 (7–35)	98 (97–99)
S05	24 (21–30)	15 (11–21)	97 (96–98)
S06	9 (8–11)	8 (7–10)	98 (98–98)
AVG	23	14	97
40 Hz AGF			
S02	17 (11–29)	14 (10–22)	98 (97–99)
S04	10 (7–12)	8 (6–10)	99 (99–99)
S07	15 (5–35)	7 (3–15)	69 (11–99)
S08	14 (11–19)	12 (10–17)	99 (99–99)
S09	20 (14–24)	18 (12–23)	99 (98–99)
S10	17 (13–19)	14 (9–18)	98 (94–99)
S11	22 (12–28)	12 (9–15)	98 (97–99)
AVG	16	12	96

The change in neural background noise level and the number of rejected ICs again indicate that the ICA separation is not perfect in many cases. In [15], the authors mention that 'experts may ignore noise related ICs contaminated with residual CI artifact(s) since these normally explain a small amount of variance in the AEPs'. This suggests that improper separation of neural background noise and CI artifacts is also a problem for transient evoked potentials, complementary to our observations for EASSRs.

As an alternative to the ICA decomposition on all recorded channel signals, two additional approaches were developed and evaluated for (a selection of subjects in) the MFTF40 dataset. In the first approach, fewer recording channels, i.e. 32 (ICA32) or 48 (ICA48) channels, are used for the ICA decomposition. ICs containing the same activity may be collapsed into one when fewer recording channels are used. The same results were obtained with ICA32 and ICA48, compared to ICA, for most subjects. The average number of rejected ICs is 10 (31%), 11 (26%) and 12 (21%), for ICA32, ICA48 and ICA, respectively. The minimum (maximum)

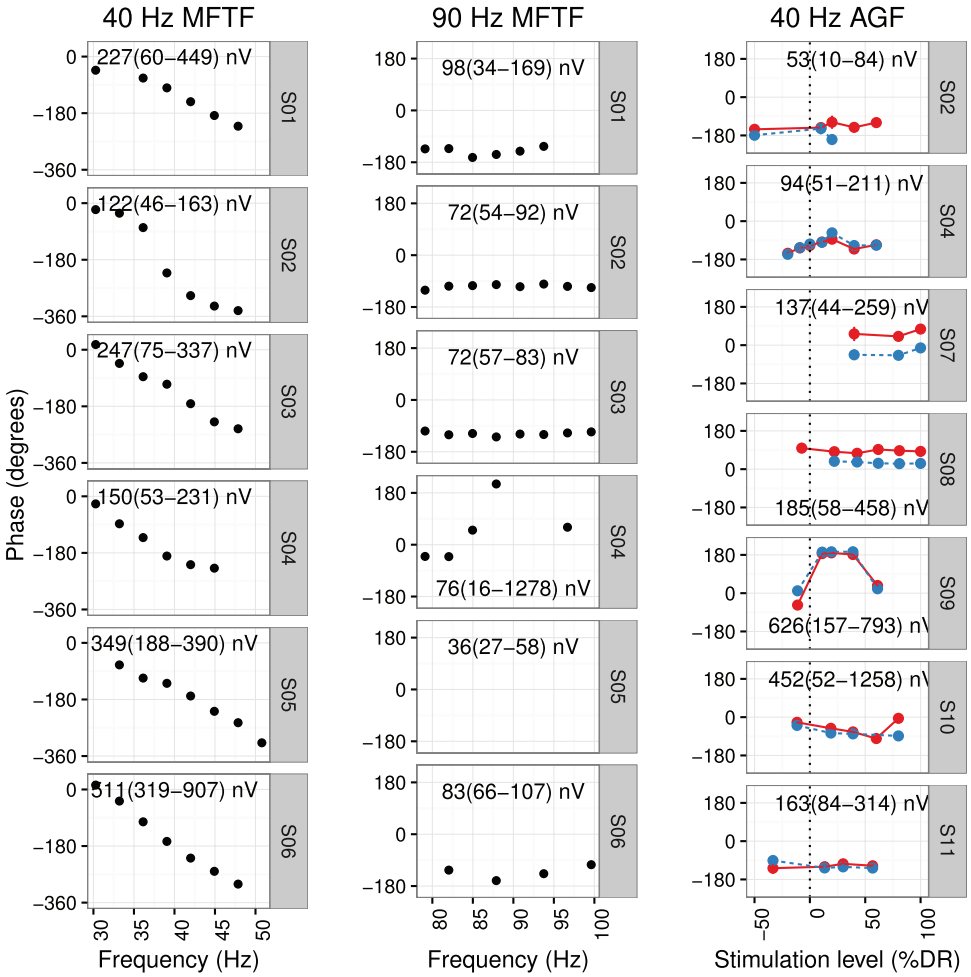


Figure 11. $\theta_{NO}^{r,C}$ as a function of f_m (40 and 90 Hz MFTF dataset) or stimulation level (40 Hz AGF dataset) without CI artifacts attenuation, in the mean *contralateral* channel. The dataset is indicated on top. The range and median value of $A_{NO}^{r,C}$ (vector summation of CI artifacts and EASSR) are included as text. No data points are shown for S05 for the 90 Hz MFTF dataset, as only data points with significant synchronous activity are included. Together, amplitude and phase suggest whether the recording is CI artifacts or EASSR dominated. When signals are EASSR dominated in contralateral recording channels, ICA seems to separate the sources good enough to result in adequate CI artifacts attenuation.

number of rejected ICs is 4 (20), 5 (27), and 5 (28) for ICA32, ICA48 and ICA, respectively. Furthermore, the percentage of rejected ICs increased when fewer recording channels were used for the ICA decomposition. In the second approach, a LI was applied to the recorded channel signals prior to ICA decomposition (LI+ICA). LI may reduce the CI artifacts amplitude, which could result in a better ICA decomposition. On the other hand, the LI introduces artificial dependencies between the channel signals. ICs representing CI artifacts were then manually identified, because LI distorts the relation between the spectral CI artifacts amplitude at f_m and f_c. While synchronous response phases were mostly similar for ICA and LI+ICA, significant differences in synchronous response amplitude between ICA and LI+ICA were observed for almost all frequencies, in all subjects and in both hemispheres. LI+ICA does not seem to improve the quality of the ICA decomposition, not even for the dataset where ICA seemed successful. It cannot be ruled out that different IC selection criteria would provide better results. However, even if the LI+ICA method would work well, the need for manual IC identification is a serious disadvantage.

4.2. Limitations

In this study, only one ICA algorithm, Infomax ICA, has been used. Many reports indicate that Infomax ICA is the most successful ICA algorithm to separate EEG and artifactual sources [14, 15, 33, 41–43]. This study only aimed to assess the baseline performance of ICA in attenuating CI artifacts, not to find the best ICA algorithm. Furthermore, the algorithm was evaluated using the default settings. Again, since this study aims to evaluate baseline ICA performance for CI artifacts attenuation, optimizing the parameter set was outside the scope of the study.

The selection of ICs associated with CI artifacts was automated using a heuristic measure, by comparing the spectral amplitude at f_c to a predetermined threshold. The value of this threshold was determined by trial and error, and is merely used to create an objective IC selection method. Most probably, better alternatives exist. This study showed that ICA is not capable of completely separating EASSR, CI artifacts, ocular, or muscle artifacts, and neural background noise. Therefore, the optimal setting of the IC selection threshold is

not critical for the performance of the method, that is already compromised by the sometimes poor separation quality.

4.3. Significance

We have shown that the ICA method is only able to sufficiently attenuate CI artifacts for the 40 Hz MFTF dataset. We hypothesize that the ICA separation quality depends on whether the contralateral hemisphere is CI artifacts dominated prior to CI artifacts attenuation. This hypothesis could possibly be verified using simulations, by artificially adding a modeled CI artifacts signal and EASSR. Simulations lack the authenticity of real EEG measurements, and assumptions, e.g. about CI artifacts propagation, and EASSR source location, have to be imposed. Within a subject, for fixed stimulation parameters, it is not possible to manipulate the location or the distribution of the EASSR or the CI artifacts. Therefore, we cannot systematically investigate the influence of EASSR and CI artifacts distribution on the ICA separation quality intra-subject.

Although the ICA does not attenuate CI artifacts below the neural noise level for all tested conditions, we showed that EASSR dominated signals can be obtained in ipsilateral recording channels for the 40 Hz MFTF dataset. Attenuating CI artifacts in ipsilateral channels is crucial for source localization and testing subjects with bilateral CI stimulation.

5. Conclusion

This study aimed to evaluate the performance of an ICA based CI artifacts attenuation method on three datasets containing EASSRs. Results indicate that the separation quality of the ICA depends on the CI artifacts present in the contralateral hemisphere. For the 40 Hz MFTF dataset containing large EASSRs, ICA was capable of removing CI artifacts from all ipsilateral recording channels, without distorting the EASSR in the mean contralateral channel. In the 90 Hz MFTF dataset, EASSR were smaller or absent, and results obtained with ICA were inconsistent. In the 40 Hz AGF dataset, the stimulation level was varied from a subthreshold level to comfort level, covering a whole range of EASSR amplitudes. Good results were obtained for two subjects with large 40 Hz EASSRs and minor CI artifacts in the contralateral hemisphere. For the remaining five subjects, recordings were CI artifacts dominated in the contralateral hemisphere, due to small EASSRs or large CI artifacts. Neural background noise levels were greatly reduced after ICA compared to NO, indicating that ICA did not succeed in perfectly separating neural background noise and CI artifacts (and possibly EASSR). Furthermore, a large number of ICs was rejected in most recordings, whereas it was expected that the CI artifacts would be expressed in a limited number of ICs in case of perfect separation. In conclusion, the relative contribution of CI artifacts and EASSR in the contralateral recording channels seems to be important for the ICA separation quality. Despite the success of ICA based CI artifacts attenuation for transient responses, it was found to be only successful in a limited number of cases for steady-state responses.

Acknowledgment

The authors would like to thank all CI recipients that participated in this research. Special thanks goes to Robert Luke and Tom Francart for their valuable input and feedback on this work.

This research work was carried out in the frame of Research Project FWO nr. G.066213 'Objective mapping of cochlear implants', and IWT O&O Project nr. 150432 'Advances in Auditory Implants: Signal Processing and Clinical Aspects'. The second author is supported by a PhD grant by the Hermes fund (141243).

ORCID iDs

Hanne Deprez https://orcid.org/0000-0001-9784-2826

References

[1] Wouters J, McDermott H J and Francart T 2015 Sound coding in cochlear implants: from electric pulses to hearing *IEEE Signal Process. Mag.* **32** 67–80
[2] Zwolan T A, Kileny P R, Ashbaugh C and Telian S A 1996 Patient performance with the Cochlear Corporation '20 + 2' implant: bipolar versus monopolar activation *Am. J. Otol.* **17** 717–23
[3] Brown C J, Hughes M L, Luk B, Abbas P J, Wolaver A and Gervais J 2000 The relationship between EAP and EABR thresholds and levels used to program the nucleus 24 speech processor: data from adults *Ear Hear.* **21** 151–63
[4] Hofmann M and Wouters J 2012 Improved electrically evoked auditory steady-state response thresholds in humans *J. Assoc. Res. Otolaryngol.* **13** 573–89
[5] Hofmann M and Wouters J 2010 Electrically evoked auditory steady state responses in cochlear implant users *J. Assoc. Res. Otolaryngol.* **11** 267–82
[6] Gilley P, Sharma A and Dorman M 2008 Cortical reorganization in children with cochlear implants *Brain Res* **1239** 56–65
[7] Gordon K, Wong D and Papsin B 2013 Bilateral input protects the cortex from unilaterally-driven reorganization in children who are deaf *Brain* **136** 1609–25
[8] Gordon K, Henkin Y and Kral A 2015 Asymmetric hearing during development: the aural preference syndrome and treatment options *Pediatrics* **136** 141–53
[9] Sharma A, Dorman M F and Spahr A J 2002 A sensitive period for the development of the central auditory system in children with cochlear implants: implications for age of implantation *Ear Hear.* **23** 532–9
[10] Sharma A, Gilley P, Dorman M F and Baldwin R 2007 Deprivation-induced cortical reorganization in children with cochlear implants *Int. J. Audiol.* **46** 494–9
[11] Sharma A, Nash A and Dorman M F 2009 Cortical development, plasticity and re-organization in children with cochlear implants *J. Commun. Disorders* **42** 272–9
[12] Miller C, Brown C, Abbas P and Chi S 2008 The clinical application of potentials evoked from the peripheral auditory system *Hear. Res.* **242** 184–97
[13] Gilley P, Sharma A, Dorman M, Finley C, Panch A and Martin K 2006 Minimization of cochlear implant stimulus artifact in cortical auditory evoked potentials *Clin. Neurophysiol.* **117** 1772–82
[14] Viola F, Thorne J, Bleeck S, Eyles J and Debener S 2011 Uncovering auditory evoked potentials from cochlear

implant users with independent component analysis *Psychophysiology* **48** 1470–80
[15] Viola F, De Vos M, Hine J, Sandmann P, Bleeck S, Eyles J and Debener S 2012 Semi-automatic attenuation of cochlear implant artifacts for the evaluation of late auditory evoked potentials *Hear. Res.* **284** 6–15
[16] Wong D and Gordon K 2009 Beamformer suppression of cochlear implant artifacts in an electroencephalography dataset *IEEE Trans. Biomed. Eng.* **56** 2851–7
[17] Gransier R, Deprez H, Hofmann M, Moonen M, van Wieringen A and Wouters J 2016 Auditory steady-state responses in cochlear implant users: effect of modulation frequency and stimulation artifacts *Hear. Res.* **335** 149–60
[18] Picton T, John M, Dimitrijevic A and Purcell D 2003 Human auditory steady-state responses: respuestas auditivas de estado estable en humanos *Int. J. Audiol.* **42** 177–219
[19] Hotelling H 1931 The generalization of student's ratio *Ann. Math. Stat.* **2** 360–78
[20] Dobie R and Wilson M 1996 A comparison of t test, F test and coherence methods of detecting steady-state auditory-evoked potentials, distortion-product otoacoustic emissions, or other sinusoids *J. Acoust. Soc. Am.* **100** 2236–46
[21] McKay C, Fewster L and Dawson P 2005 A different approach to using neural response telemetry for automated cochlear implant processor programming *Ear Hear.* **26** 38S–44S
[22] McKay C, Lim H and Lenarz T 2013 Temporal processing in the auditory system: insights from cochlear and auditory midbrain implantees *J. Assoc. Res. Otolaryngol.* **14** 103–24
[23] Hughes M, Brown C, Abbas P, Wolaver A and Gervais J 2000 Comparison of EAP thresholds with MAP levels in the Nucleus 24 cochlear implant: data from children *Ear Hear.* **21** 164–74
[24] Deprez H, Gransier R, Hofmann M, van Wieringen A, Wouters J and Moonen M 2017 Characterization of cochlear implant artifacts in electrically evoked auditory steady-state responses *Biomed. Signal Process. Control* **31** 127–38
[25] Li X, Nie K, Karp F, Tremblay K and Rubinstein J 2010 Characteristics of stimulus artifacts in EEG recordings induced by electrical stimulation of cochlear implants *3rd Int. Conf. on Biomedical Engineering and Informatics* (IEEE) pp 799–803
[26] Hughes M, Brown C and Abbas P 2004 Sensitivity and specificity of averaged electrode voltage measures in cochlear implant recipients *Ear Hear.* **25** 431–46
[27] Heffer L and Fallon J 2008 A novel stimulus artifact removal technique for high-rate electrical stimulation *J. Neurosci. Methods* **170** 277–84
[28] Luke R and Wouters J 2016 Kalman filter based estimation of auditory steady state response parameters *IEEE Trans. Neural Syst. Rehabil. Eng.* **25** 196–204
[29] Deprez H, Gransier R, Hofmann M, van Wieringen A, Wouters J and Moonen M 2016 Template subtraction to remove CI stimulation artifacts in auditory steady-state responses in CI subjects *IEEE Trans. Neural Syst. Rehabil. Eng.* **25** 1322–31
[30] Deprez H, Hofmann M, van Wieringen A, Wouters J and Moonen M 2014 Cochlear implant artifact rejection in electrically evoked auditory stead y state responses *22nd European Signal Processing Conf.* pp 1995–9
[31] Castaneda-Villa N and James C J 2007 Objective source selection in blind source separation of AEPs in children with cochlear implants *Annu. Int. Conf. of the IEEE Engineering in Medicine and Biology* (IEEE) pp 6223–6
[32] Castaneda-Villa N and James C 2008 The selection of optimal ICA algorithm parameters for robust AEP component estimates using 3 popular ICA algorithms *Annu. Int. Conf. of the IEEE Engineering in Medicine and Biology Society* pp 5216–9
[33] Debener S, Hine J, Bleeck S and Eyles J 2008 Source localization of auditory evoked potentials after cochlear implantation *Psychophysiology* **45** 20–4
[34] Castaneda-Villa N and James C 2011 Independent component analysis for auditory evoked potentials and cochlear implant artifact estimation *IEEE Trans. Biomed. Eng.* **58** 348–54
[35] Sandmann P, Eichele T, Buechler M, Debener S, Jäncke L, Dillier N, Hugdahl K and Meyer M 2009 Evaluation of evoked potentials to dyadic tones after cochlear implantation *Brain* **132** 1967–79
[36] Sandmann P, Kegel A, Eichele T, Dillier N, Lai W, Bendixen A, Debener S, Jancke L and Meyer M 2010 Neurophysiological evidence of impaired musical sound perception in cochlear-implant users *Clin. Neurophysiol.* **121** 2070–82
[37] Martin B 2007 Can the acoustic change complex be recorded in an individual with a cochlear implant? separating neural responses from cochlear implant artifact *J. Am. Acad. Audiol.* **18** 126–40
[38] Bakhos D, Roux S, Robier A, Bonnet-Brilhault F, Lescanne E and Bruneau N 2012 Minimization of cochlear implant artifact in cortical auditory evoked potentials in children *Int. J. Pediatric Otorhinolaryngol.* **76** 1627–32
[39] Miller S and Zhang Y 2014 Validation of the cochlear implant artifact correction tool for auditory electrophysiology *Neurosci. Lett.* **577** 51–5
[40] Delorme A and Makeig S 2004 EEGLAB: An open source toolbox for analysis of single-trial EEG dynamics including independent component analysis *J. Neurosci. Methods* **134** 9–21
[41] Delorme A, Sejnowski T and Makeig S 2007 Enhanced detection of artifacts in EEG data using higher-order statistics and independent component analysis *NeuroImage* **34** 1443–9
[42] Debener S, Thorne J, Schneider T and Viola F 2010 Using ICA for the analysis of multi-channel EEG data *Simultaneous EEG and fMRI: Recording, Analysis and Application* (Oxford: Oxford University Press) pp 121–33
[43] Delorme A, Palmer J, Onton J, Oostenveld R and Makeig S 2012 Independent EEG sources are dipolar *PLoS One* **7** e30135
[44] Luke R, Van Deun L, Hofmann M, Van Wieringen A and Wouters J 2015 Assessing temporal modulation sensitivity using electrically evoked auditory steady state responses *Hear. Res.* **324** 37–45
[45] McMenamin B W, Shackman A J, Maxwell J S, Bachhuber D R W, Koppenhaver A M, Greischar L L and Davidson R J 2010 Validation of ICA-based myogenic artifact correction for scalp and source-localized EEG *NeuroImage* **49** 2416–32